Reliability Assessment of Multistate Degraded Systems: An Application to Power Electronic Systems

Vahid Samavatian, Hossein Iman-Eini, *Senior Member, IEEE*, and Yvan Avenas

***Abstract*—This article demonstrates the feasibility of using a multistate degraded system analysis for obtaining much more accuracy in reliability evaluation. The proposed method is capable of estimating system-level reliability, while mission profile and physics of failure of the system's items are taken into account. In addition, the self and mutual degradation effects of items on the operation of the global system have been considered. Not only does the proposed framework can be employed in determining the reliability of the degraded systems in terms of multistate functions, but also obtains the states of the systems by estimating the system state probabilities. As an application, a power electronic system containing three critical items has been studied. In this case study, two power semiconductors and a capacitor have been considered as three degradation processes and their aging effects on the useful lifetime estimation of the power electronic system has been discussed.**

***Index Terms*—Lifetime estimation, multistate degraded systems, power electronic systems, reliability.**

I. Introduction

A CONVENTIONAL binary-state reliability model in which only two possible states, namely perfectly functioning and complete failure, are assumed for a system and its components are inadequate to present the multistate inherent of complicated engineered systems [1]–[3]. In many real engineered applications, particularly power electronic systems, there exist several intermediate states for characterizing health of the systems [4], [5]. Therefore, a multistate system model is able to manifest the sophisticated degrading (aging) behaviors of the engineered system beyond the binary-state model [6]–[9].

The deteriorating process of a component or a system may be accelerated owing to aging. Accordingly, static reliability assessment has not been able to estimate the reliability of a system [10]. A dynamic reliability assessment method for a multistate system through the aggregation of multilevel inspection data is developed [11], [12]. In these studies, the state of a system is extracted owing to the imperfections of inspections. The inspection data are able to be simultaneously or asynchronously gathered across multiple levels of the system. Although the reliability function of the system can be dynamically updated, this method is unable to address the cases in which an inspector is related to multiple components, which is the case in engineered systems.

Stochastic processes [13], [14], extended the decision diagram-based methods [15]–[17] and the universal generating functions [18], [19] have proposed some frameworks for dynamic reliability assessment in which the failure rate of items have been considered time dependent. Although the model is capable of considering degradation dependencies, its implementation for the higher number of components is complicated and time consuming. Furthermore, they are failing to consider the mission profile of the system.

Liu *et al.* [20] proposed a new reliability model for the multistate systems with state transition dependency. They used copula functions to characterize the dependence among state transitions and to construct a multivariate distribution. Huge computational burden owing to the high-dimensional integration in the likelihood function and more unknown parameters is the main detriment of this approach.

In order to attain the reliability specifications and risk functions of the multistate systems, an approach based on an inverse L_z transform is proposed by Lisnianski and Ding [21]. However, the dependence of system components is not taken into account. Song *et al.* [22] proposed the stochastic multivalued models for evaluating the reliability of a multistate system with dependent multistate components. The major defect in this method is the difficulty of precise performance estimation of the multistate components due to the challenges associated with the probability of the state's determination.

A multilayered vector-valued continuous-time Markov chain was utilized to obtain a stochastic dependency [20] among multistate components in [23] and [24] and an aggregated Markov process was employed to mitigate the computational complexity resulting from system reliability evaluation. However, its inability to take into account the self-degradation of components and lack of consideration of mission profile and failure root causes are the detriments of this method.

Failure to consider mission profile of the system, inability to take into account the mutual and self-degradation effects (dependencies) on the performance of system, inability to use deterministic knowledge (i.e., physics of failure (PoF) which is necessary for design for reliability in the engineering systems), and inability to correlate components states to the system states that may simplify the extraction of the data inspection and

Manuscript received February 2, 2019; revised March 31, 2019 and June 5, 2019; accepted July 28, 2019. Date of publication August 4, 2019; date of current version January 10, 2020. Recommended for publication by Associate Editor T. M. Lebey. *(Corresponding author: Hossein Iman-Eini.)*

V. Samavatian is with the School of Electrical and Computer Engineering, College of Engineering, University of Tehran, Tehran 14399-57131, Iran, and also with Grenoble INP, Université Grenoble Alpes, CNRS, Grenoble 38000, France (e-mail: vahidsamavatian@ut.ac.ir).

H. Iman-Eini is with the School of Electrical and Computer Engineering, College of Engineering, University of Tehran, Tehran 14399-57131, Iran (e-mail: imaneini@ut.ac.ir).

Y. Avenas is with the Grenoble INP, Université Grenoble Alpes, CNRS, Grenoble 38000, France (e-mail: yvan.avenas@g2elab.grenoble-inp.fr).

Color versions of one or more of the figures in this article are available online at http://ieeexplore.ieee.org.

Digital Object Identifier 10.1109/TPEL.2019.2933063

See http://www.ieee.org/publications_standards/publications/rights/index.html for more information.

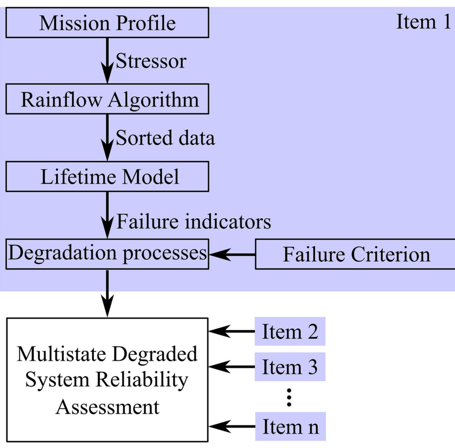

Fig. 1. Global flowchart of reliability assessment of an n-component system.

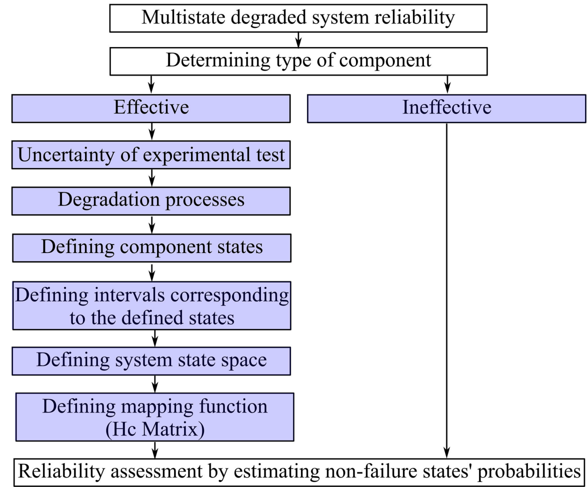

Fig. 2. Analysis procedure of a multistate degraded system (see Fig. 1).

complexity of implementation are the detriments of the aforementioned studies posing considerable challenges in reliability assessment of the multistate degraded systems.

To bridge above gap, a novel PoF-based reliability assessment framework is proposed in this article. This method converts a dependent system to a multistate independent system by discretizing the global system states to the specific state space. In each state of the global system, detached operating conditions are assumed. In the proposed method, the mission profile of the undertaken system has been considered, as shown in Fig. 1. The translated mission profile has been applied to the Rainflow algorithm in order to sort the complex data to the understandable data. The sorted data are also applied to the lifetime model of an item. The output of the lifetime model is one or more failure indicators. The trends of failure indicators have been curve fitted and finally applied to the main multistate degraded system reliability assessment. Based on the failure criterion of each item and its corresponded degradation levels, a state for the system will be defined. Accordingly, a multistate system is defined based on the items' degradation states.

The remainder of this article is as follows. Section II puts forward the newly proposed multistate degraded system reliability assessment. Section III deals with the proposed method's application to the power electronic system and expressing experimental procedure. While results and discussion are presented in Section IV, a conclusion is drawn in Section V.

II. Multistate Degraded Systems

A multistate degraded system analyzing flowchart is shown in Fig. 2. Based on the field experiences and analytic investigation, one can divide the components into two different categories, namely effective and ineffective. Effective items' degradation directly affects the system reliability by changing its state. However, it is not the case in the ineffective components. These items directly cause the system to the failure state provided that they reach to their failure criteria. Regarding this figure, degradation processes of system's components and their uncertainties are applied to the effective items in which their degradations affect the system state. For effective components, different functional states as well as their corresponding intervals are defined. Then the system functional state space and the mapping function (H_C matrix) between the components states and system states are defined. Finally, one can estimate system reliability by assessing nonfailure system states' probabilities and reliability of ineffective as well.

A. System Description

A system can be constituted by several subsystems or items that are exposed to various failure processes. In a reliability point of view, some important issues have to be considered: 1) the degradation of every item does not follow a constant trend (constant failure rate) due to the wearing out manner, which is also accelerated by aging; 2) the degradations of different items can affect the degradation process of the other items by changing the operational point of the considered system; and 3) mission profile does play a central role on the wearing out behavior of the items. Accordingly, the degradation trends (process) of the items have to be considered based on the mission profile. In addition, by dividing different system degraded states (new operational points), the effect of mutual and self-degradations of the items in the system will be considered. The degradation process of effective items is considered as a function of time and is denoted by $Y_i(t)$, $i = 1, 2, \ldots, k$. However, the degradation of ineffective items does not affect the system operating points (system state). Therefore, there is no need of considering degradation processes and only their complete failures ($D_\ell(t)$, $j = 1, 2, \ldots, \ell$) can affect the system's failure. k and ℓ are the number of effective and ineffective items, respectively, (also $k + \ell = n$, where n is the total number of items in the global systems).

Since every item is initially in its perfect states M_i, the global system is also being in its perfect state. By time passing (aging), the effective items may reach either another degraded state, namely $(M-1)_i$, or system failed state (F). After degradation, the item can reach the other state, namely $(M-2)_i$ or failure state. A transition may be occurred from any system states to the failure state whenever an ineffective item fails owing to the random shock which is subjected to.

The degradation process may continue and passed all the aging stages till the last degradation state, i.e., 0_k reaches. If the system reaches the last degradation state, there is an imperfection in the functionality of the system, and the system must be considered as a failure (state 0). Fig. 3 demonstrates the system block diagram of the multiple competing degradation processes including effective and ineffective items. In Fig. 3, the above part presents the degradation process of effective

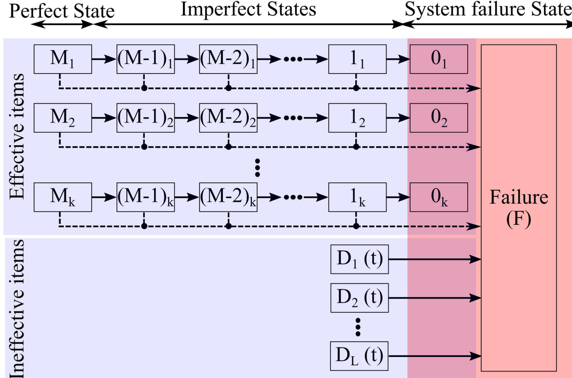

Fig. 3. Block diagram of the *n*-component system subjected to multiple failure processes.

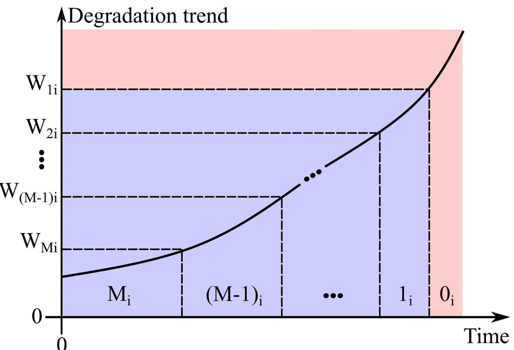

Fig. 4. Degradation process and states and their corresponding intervals.

items (components) and the bottom part presents the degradation process of ineffective items. While ineffective items may directly lead to the catastrophic failure owing to the mission profile they are exposed to, the degradation processes of the effective items may lead an item to transmit from healthier state to either the more degraded states or the catastrophic failure state. Although the system can continue working during the degraded states, it does not work in the perfect state. Thereby, some imperfect states have to be defined for the system, as shown in Fig. 3.

B. Method Assumptions

Some assumptions in formulating this newly proposed method have been defined as follows.

1) The system consists of $M + 2$ states in which state 0 and state F are both complete failure states. State 0 represents that the degradation threshold has been exceeded and state F demonstrates a complete (catastrophic) failure occurred by ineffective items or sudden defects in the effective items as shown in Fig. 3.
2) It is assumed that there is no repair and maintenance performing on the system (system is nonrepairable).
3) It is assumed that degradation processes of effective items, i.e., $Y_i(t)$, are nonnegative, strictly nondecreasing functions at time t owing to irreversible accumulation of damages.
4) It is assumed that $Y_i(t)$, $i = 1, 2, \ldots, k$ and $D_j(t)$, $j = 1, 2, \ldots, \ell$ are statistically independent. It means that the degradation process of one item in its specific state does not have an effect on the others.
5) The system is in the perfect state at time $t = 0$.
6) The system may fail either owing to the each effective degradation process, i.e., $Y_i(t) > G_i$, $i = 1, 2, \ldots, k$ or owing to each ineffective degradation process, e.g., $D_j(t;\eta,\beta) \sim W_j(\eta,\beta) > B_{sj}$, $j = 1, 2, \ldots, \ell$, where G_i and S_j are the critical values for the effective degradation processes and threshold value in which the probability of failure process will reach a specified point S_j for ineffective items, respectively.
7) The critical value G_i depends upon the function of the intermediate degradation states of the systems.

C. Methodology

As it was mentioned, the degradations of different effective items can affect the degradation processes of the other items by changing the operational point of the system. For example, by degradation of item 1, some of its critical values will vary that can change the operating point of the system and lead to accelerated aging of the other items. This accelerated aging caused by the other items has been called mutual degradation effects. This operating point change can also accelerate item 1 degradation. This accelerated aging caused by the item itself has been called self-degradation effects.

1) Formulating Effective Degradation Processes in Terms of Discrete State Space Sets: The k effective degradation processes have been considered here. For each of them, a finite number of different discrete states has also been taken into account. The state space is denoted by $\boldsymbol{\Omega}_i = \{M_i, (M-1)_i, \ldots, 1_i, 0_i\}$, $i = 1, 2, \ldots, k$ corresponding to the degradation process i with $M_i + 1$ states. M_i, $i = 1, 2, \ldots, k$ may or may not be the same and $M_i < \infty$.

Degradation processes are defined by the finite number of states. As an example, $Y_i(t)$ falls into the predefined intervals corresponding to the specified intermediate degradation states.

Let define the intervals as follows: $[0, W_{Mi}]$, $(W_{Mi}$, $W_{(M-1)i}]$, $\ldots$, $(W_{2i}, W_{1i}]$ where $W_{Mi} > W_{(M-1)i} > W_{(M-2)i} > \cdots > W_{1i}$, as shown in Fig. 4. W_i is the intermediate threshold value for the ith degradation process. Fig. 4 demonstrates a sample degradation trend. As it is clearly observed, the degradation trend follows an accelerated strict-increasing pattern. Intervals are, respectively, corresponding to the intermediate degradation states as M_i, $(M-1)_i$, $\ldots$, 1_i, 0_i.

Mathematically, one can find the relationship between the degradation process states and their corresponding intervals as expressed in (1) as follows:

Effective degradation process state

$$\begin{aligned}
&0 < Y_i(t) \le W_{Mi} && \Rightarrow\ M_i\\
&W_{Mi} < Y_i(t) \le W_{(M-1)i} && \Rightarrow\ (M-1)_i\\
& && \vdots\\
&W_{2i} < Y_i(t) \le W_{1i} && \Rightarrow 1_i\\
&G_i = W_{1i} < Y_i(t) && \Rightarrow 0_i.
\end{aligned} \tag{1}$$

2) System State Space: System state space is defined as $\boldsymbol{\Omega}_U = \{M, \ldots, 1, 0, F\}$ considering $M + 2$ distinct states. In this section, a relationship between the effective degradation processes $\{\boldsymbol{\Omega}_i, F\}$, $i = 0, 1, \ldots, k$ and the global system state space $\boldsymbol{\Omega}_U$ will be established. It is assumed that the system is not in its catastrophic failure state (F) at the time t. Therefore,

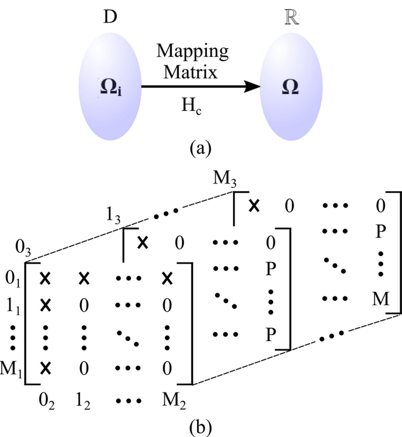

Fig. 5. Mapping matrix. (a) Each state of effective items is allocated to a specific global system state. (b) Three-item mapping matrix H_c where $P\epsilon\mathbf{\Omega} = \{M-1,\ M-2,\ \ldots,\ 1\}$.

one can cross out the state F from the global system state space. Thus, a correlation between $\mathbf{\Omega}$ and $\mathbf{\Omega}_i$ is required instead of a correlation between $\mathbf{\Omega}_U$ and $\{\mathbf{\Omega}_i,\ F\},\ i = 0,\ 1,\ \ldots,\ k$.

A mapping function has to be defined for relating these two different sets as f: $\mathbb{R} = \mathbf{\Omega_1} \times \mathbf{\Omega_2} \times \cdots \times \mathbf{\Omega_k} \rightarrow \mathbf{\Omega} = \{M, M-1,\ \ldots,\ 1,\ 0\}$ where $\mathbb{R} = \mathbf{\Omega_1} \times \mathbf{\Omega_2} \times \cdots \times \mathbf{\Omega_k} = \{(i_1, i_2, \ldots, i_k) | i_1 \epsilon \mathbf{\Omega_1}, i_2 \epsilon \mathbf{\Omega_2}, \ldots, i_k \epsilon \mathbf{\Omega_k}\}$ is a Cartesian product as the input space domain, and shown in Fig. 5. The domain and the range of the mapping function have been indicated in Fig. 5(a). H_c is the mapping matrix with the dimensions of $(M_1+1) \times (M_2+1) \times \cdots \times (M_k+1)$ in which M_i is the number of probable states for the ith effective items and $i =$ 0,1, …, k. For example, for $k = 3$, a three-dimensional (3-D) mapping matrix is required. Thereby, the first item constitutes the rows of the mapping matrix, the second one constitutes the column of the mapping matrix, and the third one constitutes the pages of the matrix, as shown in Fig. 5(b). Mapping matrix of H_c has mapped the different input states to the specific output global states containing $M + 1$ distinct states.

While different rows of mapping matrix H_c are allocated to different intermediate degradation states of the first item, different columns and pages are allocated to the second and the third items, respectively. The elements of H_c represent $f(i_1, i_2, \ldots, i_k) = P$ in which $i_1 \epsilon \mathbf{\Omega_1}$, $i_2 \epsilon \mathbf{\Omega_2}, \ldots, i_k \epsilon \mathbf{\Omega}_k$ and $P \epsilon \{M-1,\ M-2,\ \ldots,\ 1\}$. Regarding Fig. 5(b), the first elements of mapping matrix H_c in whole the matrix pages and the first column and the first row of the first mapping matrix page as well have been demonstrated by $\times$. These elements are not achievable, because if one of the items reach its failure state (0_i), the system stops working and necessarily the others cannot reach their failure states as well. All the other elements in the first page, in which the third element is in its failure state (0_3), are equal to zero. In addition, for all the matrix pages, the first rows and the first columns (except the first element) are also zero due to the zero states of the first and the second items degradation states. The last element of mapping matrix H_c is the perfect state of the global system (M) in which the system is initially in it because all the effective items are in their healthy (perfect) states. The other elements in H_c are imperfect states belonging to the global state system $\mathbf{\Omega}$ except M, namely global system perfect state. Some other elements also may be considered zero when the items are in their low states. It means that in the states in which some of the effective items are roughly degraded, one can define those states as the global degraded states.

Time-to-failure of the global system is defined as follows:

$$T = \inf\{t : Y_i(t) > G_i,\ i = 1, 2, \ldots, k \text{ or } F_j > B_{S_j}\ \ j = 1, 2, \ldots, \ell\}. \tag{2}$$

All the degradation processes including effective and ineffective items are competing in the reliability of the global system. However, the global system will be failed provided that the only one of the degradation processes exceeds its critical value. Accordingly, for all combinations of $Y_i(t),\ i = 1, 2, \ldots, k$ and also for all combinations of $D_j(t),\ j = 1, 2, \ldots, \ell$, following events never occurred:

$$P\left\{\begin{array}{l} Y_i(t) > G_i \quad \forall \bigcup_{ii=1}^{k, ii\neq i} Y_{ii}(t)|, \quad i = 1, 2, \ldots, k \\ D_j(t) < B(S_j)\,|, \quad j = 1, 2, \ldots, l \end{array}\right\} = 0$$

$$P\left\{\begin{array}{l} Y_i(t) < G_i|, \quad i = 1, 2, \ldots, k \\ D_j(t) > B(S_j) \quad \forall \bigcup_{jj=1}^{k, jj\neq j} D_{jj}(t)|, \quad j = 1, 2, \ldots, l \end{array}\right\} = 0$$

$$P\left\{\begin{array}{l} Y_i(t) > G_i \quad \forall \bigcup_{ii=1}^{k, ii\neq i} Y_{ii}(t)|, \ i = 1, 2, \ldots, k, \\ D_j(t) > B(S_j) \quad \forall \bigcup_{jj=1}^{k, jj\neq j} D_{jj}(t)|, \quad j = 1, 2, \ldots, l \end{array}\right\} = 0. \tag{3}$$

It means that if one of the effective or ineffective items reaches its failure state, the global system will fail and thereby the combination of the other items in their failure states will never happen. Thus, the probability of any combination of the failure states of effective and ineffective items becomes zero.

The function f: $\mathbb{R} = \mathbf{\Omega_1} \times \mathbf{\Omega_2} \times \cdots \times \mathbf{\Omega_k} \rightarrow \mathbf{\Omega} = \{M, M-1,\ \ldots,\ 1,\ 0\}$ has to meet the following requirements:

1) $f(M_1,\ M_2,\ \ldots,\ M_k) = M$ and $f(0_1,\ a_2,\ \ldots,\ a_k) = f(a_1,\ 0_2,\ \ldots,\ a_k) = f(a_1,\ a_2,\ \ldots,\ 0_k) = 0$, where $a_i\, \epsilon \mathbf{\Omega}_i,\ i = 1,\ 2,\ \ldots,\ k$.
2) f is a monotonic strictly nondecreasing function for each argument. For example,

$$\begin{array}{ll} f(a_1,\ a_2,\ \ldots,\ a_k) \geq f(b_1,\ a_2,\ \ldots,\ a_k), & \text{if } a_1 \geq b_1 \\ f(a_1,\ a_2,\ \ldots,\ a_k) \geq f(a_1,\ b_2,\ \ldots,\ a_k), & \text{if } a_2 \geq b_2 \\ \vdots & \\ f(a_1,\ a_2,\ \ldots,\ a_k) \geq f(a_1,\ a_2,\ \ldots,\ b_k), & \text{if } a_k \geq b_k \end{array} \tag{4}$$

where a_i and $b_i\, \epsilon \mathbf{\Omega}_i,\ i = 1,\ 2,\ \ldots,\ k$.

In real applications, a different degradation state combination can generate the same outputs. Thereby, in the mapping matrix H_c, there may be the same outputs in the different elements. Following definition has to be considered for explaining this similarity in the mapping matrix.

Definition: The ith equivalent category R_i is defined as

$$R_m = \left\{\begin{array}{r} (a_1,\ a_2,\ \ldots,\ a_k) \ \text{ where } a_1 \in \Omega_1,\ a_2 \in \Omega_2 \\ ,\ldots, a_k \in \Omega_k | f(a_1,\ a_2,\ \ldots,\ a_k) = m \end{array}\right\}$$
$$m = 0, 1, \ldots, M \tag{5}$$

where R_m demonstrates all the possible degradation state combinations that generate the global system state *m*, and R_0 and R_M are the distinct subsets dividing *R* to the $M + 1$ equivalent categories so that

$$R = \bigcup_{m=0}^{M} R_i. \tag{6}$$

D. Reliability Assessment

In this section, the probability density function and mean time to failure will be obtained on the state probabilities mentioned in Section II-C. Initially, the global system is considered to be in its perfect state, i.e., $M = f(R_M)$. The probability of being in state *M* yields by

$$P_t(M) = P_t(f(R_M)). \tag{7}$$

As defined, R_m illustrates all the possible degradation state combinations leading to the global system state of *m*. The probability of being in state *m* yields by

$$P_t(m) = P(f(R_m)). \tag{8}$$

The probability of the catastrophic failure state (*F*) is evaluated by

$$P_t(F) = P \left\{Y_i(t) \leq G_i | \, i=1,2,\ldots,k, D_j(t) \geq B(S_j) | j=1,2,\ldots,l\right\}. \tag{9}$$

The system reliability *R*(*t*) can be assessed by

$$R(t) = P\{\text{global system state} \geq 1\} = \bigcup_{m=1}^{M} P\{f(R_m)\} = \sum_{m=1}^{M} P_t(m) \tag{10}$$

where $P_t(m)$ is the probability of being in the global system state of *m*.

Assuming *T* as a continuous random variable of mean time to failure, one can calculate the mean time to failure as follows:

$$E[T] = \int_0^\infty \left\{ \prod_{i=1}^{k} P\{Y_i(t) \leq G_i\} \times \prod_{j=1}^{\ell} (F_j(\eta, \beta) < B(S_j)) \right\} dt \tag{11}$$

where F_j is the probability function of the *j*th ineffective item. The results in (11) would strongly depend on the first term in integration, i.e., effective degradation processes.

III. Application to Power Electronic Systems

In this section, we consider a power electronic system, containing various components individually confronted to different failure mechanisms. Every component has effects on the system operating conditions during its working. It has been proved that the components' degradations can extensively be effective in power electronic systems' operating points [25]. A power electronic system contains various components, which each of them may be sensitive to the various failure mechanisms leading to aging (parameter drifting). Among all the power electronic components, power semiconductors, and capacitors as well are both said to be the critical components as a reliability point of view [26].

In addition, it is notable that the power semiconductors' degradations can strongly affect the power electronic systems' electrical and thermal operating points. It was illustrated in [25] that the junction temperature of the insulated-gate bipolar transistor (IGBT) was increased from 140.3 to 170.5 °C during the aging which significantly affected the operating points of the system. However, it was not the case in the power capacitor's degradation. During capacitor aging, its parameters were considerably varied but these parameters drifting did not lead to an operating point change [25]. Although the reliability of capacitors, thereby, would be considered here, power capacitors' failure mechanisms are beyond this study and the interested readers can refer to [27].

A. Failure Mechanisms of Power Semiconductors

Regarding the critical stressors (steady-state temperature and temperature swing), the two most critical failure mechanisms are electrothermomechanical fatigue and creep [28]–[30]. Regarding physical structure of power semiconductors comprising various layers with different coefficients of thermal expansion, a meaningful set of shear and normal stresses are induced in these layers [28]. Thereby, electrothermomechanical stresses have been occurred during the power semiconductor operations leading to the plastic and elastic strains through the bodies and eventually either producing some microcracks and microvoids or growing preinduced microcracks and microvoids. The creep and creep-fatigue failures are the events activated with the rise in temperature above the one-third of melting point of metals [30]. The mentioned events are intensified upon passing of the time, when high temperature induces viscous effects to the materials. The evolution of creep damage includes the formation and growth of microvoids, microcrack formation at intergranular sites, and their coalescence in the crystals triple points [31], [32].

B. Failure Indicator of Power Semiconductors

Parameters drifting (due to degradation) plays a major role in the failure definition. In the literature, several parameters drifting has been reported [29]. However, the thermal resistance (R_{th}) is a common parameter drifting in power semiconductors and can affect device performance significantly during its aging [29].

As previously mentioned, die-attach degradation is illustrated by the crack growth and void coalescence in the solder joint. Elasto-visco-plasticitic strain in the solder joint owing to the creep-fatigue failure mechanisms is the main factor in the die-attach deterioration [33]. Since Coffin–Manson–Arrhenius lifetime model [34], [35] has been widely employed for lifetime estimation, the thermal resistance degradation processes may be expressed as follows [33]:

$$\Delta R_{\text{th}} = K \left\{ \exp\left(\frac{N}{A \times \Delta T_j{}^{\alpha} \times \exp\left(Q/RT_m\right)} \right) - 1 \right\} \tag{12}$$

where *A*, α, and *K* are both constant and device dependent, *R* and *Q* are the gas constant (8.314 $\text{JMol}^{-1}\text{K}^{-1}$) and internal energy, and T_m is the mean junction temperature of devices in Kelvin. ΔT_j expresses the junction temperature swing of devices in degree celsius. *N* is the number of cycles applied to the power semiconductors. The deterioration trend of thermal resistances, in the two mostly applied power semiconductors, i.e., IGBT and diode, was extracted from an accelerated power cycling (APC) aging test and is shown in Fig. 6. This figure demonstrates the deterioration trends of thermal resistances of the power diode and IGBT as a function of thermal cycles.

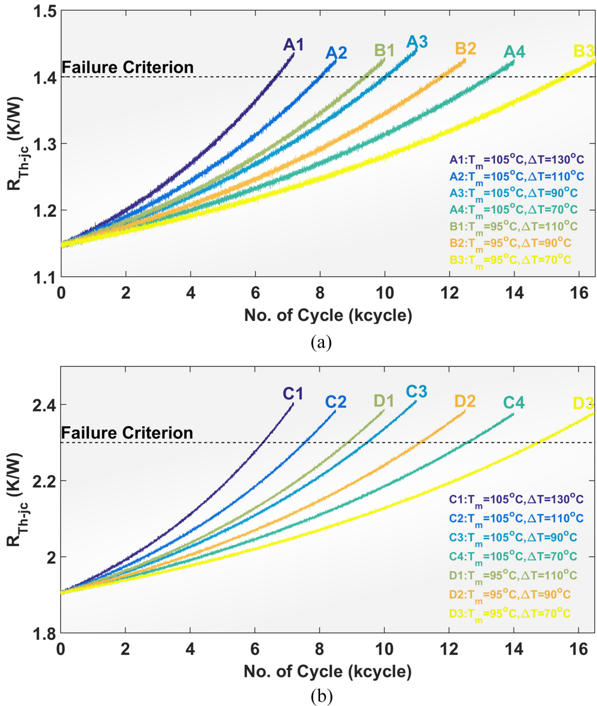

Fig. 6. Deterioration trends of power semiconductors against various thermal cycles. (a) Power IGBT. (b) Power diode.

TABLE I
IGBT NUMBER OF CYCLE TO FAILURE FOR POWER CYCLING ACCELERATED TEST

Test code	Temperature swing (°C)	T_{mean} (°C)	ΔT (°C)	Mean number of Cycles to Failure
A1	40-170	105	130	6853
A2	50-160		110	8303
A3	60-150		90	10212
A4	70-140		70	13820
B1	40-150	95	110	9825
B2	50-140		90	12233
B3	60-130		70	16102
B4	70-120		50	NA

TABLE II
DIODE NUMBER OF CYCLE TO FAILURE FOR POWER CYCLING ACCELERATED TEST

Test code	Temperature swing (°C)	T_{mean} (°C)	ΔT (°C)	Mean number of Cycles to Failure
C1	40-170	105	130	6266
C2	50-160		110	7603
C3	60-150		90	9625
C4	70-140		70	12006
D1	40-150	95	110	9051
D2	50-140		90	11208
D3	60-130		70	14864
D4	70-120		50	NA

C. Experimental Procedure

In this setup, a power current is periodically injected into the device under test (DUT) and, thereby a junction temperature swing (ΔT) is induced in the chip. Every heating up and cooling down in the junction of DUT has been defined as a distinct one power cycle. APC is continued till the failure indicators reach the defined failure criteria. The number of cycles before fulfilment of the failure criteria has been considered as a number of cycles to failure (N_F) for different temperature swing and mean temperature levels.

JESD22-A105C, JESD22-A122A, JESD22-A104E, JESD6–59B, and JESD91A are the most well-known APC testing standards. But they have never gone into much detail of the circuit design regarding different applications and various failure mechanisms. That is why various studies have been under taken by proposing their customized APC tests [35]–[38].

For obtaining the degradation processes of IGBT and power diodes, a conventional accelerated aging test has been done. In this case, IGBT and diode were exposed to cyclic thermal variations. In this study, APC aging test was employed by injecting a constant current into the IGBT and power diode. Under studied devices were 600 V–15 A IGBT and internal power diode of Infineon components, namely IKP15N60T. It has been reported that the solder layer degradation is the most probable failure site in power semiconductors [28], [29].

In this test, there were eight different conditions (different mean temperatures and temperature swings) for IGBT and power diodes. For each of them, there were four diodes and IGBTs for making the results much more accurate and reliable. Therefore, 32 IGBTs and 32 diodes were under the test.

For avoiding the catastrophic failure and changes in failure mechanism, the maximum current of 15 A was injected into the devices. This current injection led to a conduction power loss in the device which was finally leading to a temperature rise in the devices' dies. It led to a maximum temperature $T_{j\max}$. It should be noted that the devices were mounted on a cold plate with fixed temperature. Therefore, after stopping current injection, the temperature of devices decreases to the temperature of cold plate $T_{j\min}$. The relaxing time for the devices was much more to make sure that the devices' junction temperatures have reached $T_{j\min}$. This APC test had continued until device reached its failure criteria.

APC tests were performed for various mean temperatures and temperature swings for both IGBT and power diodes. The 130, 110, 90, and 70 °C temperature swings for the mean temperature of 105 °C, and 110, 70, and 70 °C for the mean temperature of 95 °C were the different conditions of APC tests for preparing number of cycles to failure degradation model (see Fig. 6).

IV. RESULTS AND DISCUSSIONS

In this section, APC results (degradation processes of IGBT and diode) are illustrated and discussed. In addition, the newly proposed reliability assessment method is applied to a specific power electronic converter as a case study in the hybrid electric vehicle as an interface between the battery bank and driving system exposed to WLTP-class3 driving cycle.

A. APC Test Results

Tables I and II list the results of the power cycling accelerated tests. In this power cycling tests, junction to case thermal resistance (as the failure indicator) had been evaluated through thermosensitive electrical parameter. It has to be mentioned that during these tests, junction to case thermal resistance exceeded the failure criterion (20% increase) [25]. It stands to reason that by solder degradation (producing voids and cracks), an increase in the junction to case thermal resistance has been led. Regarding

Tables I and II, the higher the mean temperature and temperature swing, the lower the number of cycles to failure. It is worthy to mention that for each condition, four different IGBTs/diodes had been under the test. *B*4 and *D*4 were not accessible (NA) and achieved owing to the low-temperature swing during the test.

B. Reliability Assessment

The analysis procedure applying to this case study is based on Fig. 2 and the materials explained in Section II.

1) Component Type Determination: A power converter containing two critical effective components, namely IGBT and power diode, and one critical ineffective component, namely power capacitors, has been assumed. There are three distinct items as system reliability point of view in which the system would be failed provided that one of these items is being failed. Power capacitor is considered as an ineffective item with $D(t)$ time to failure distribution following the Weibull damage model ($D(t) \sim W(\eta, \beta)$, where η and β are the scale factor and shape factor, respectively).

2) Degradation Processes of Effective Items: The degradation trends of the effective items have to be considered based on the mission profile for which the system/items are exposed to. The degradation processes of IGBT and power diode are considered as a function of time and denoted by $Y_1(t)$ and $Y_2(t)$, respectively. The degradation trends of IGBT and power diode in four different conditions have been shown in Fig. 6. These trends have been in terms of thermal cycles while they have to be in terms of time for reliability assessment. Accordingly, the WLTP-class3 driving cycle mission profile has been translated from the vehicle speed to the thermal cycling data via the power electronic electrical model, power loss model, and thermal model [25]. Then this set of complex data has been inserted to the rain flow algorithm [30] to be sorted. Finally, this set of sorted data has been applied to the Coffin–Manson–Arrhenius lifetime model [see (12)] for evaluating the degradation processes as a function of time. Based on the aforementioned procedure, one can obtain time-dependent degradation paths of IGBT and power diode as follows:

$$Y_1(t) = \begin{cases} 1.1500 + 2.246 \times 10^{-6}t & 0 < t < 25602 \text{ h} \\ 1.2075 + 2.438 \times 10^{-6}t & 25602 < t < 49194 \text{ h} \\ 1.2650 + 2.562 \times 10^{-6}t & 49194 < t < 71634 \text{ h} \\ 1.3225 + 2.812 \times 10^{-6}t & 71634 < t < 92082 \text{ h} \end{cases}$$

and

$$Y_2(t) = \begin{cases} 1.900 + 7.124 \times 10^{-6}t & 0 < t < 13336 \text{ h} \\ 1.995 + 7.189 \times 10^{-6}t & 13336 < t < 26552 \text{ h} \\ 2.090 + 7.670 \times 10^{-6}t & 26552 < t < 38912 \text{ h} \\ 2.185 + 7.740 \times 10^{-6}t & 38912 < t < 51192 \text{ h.} \end{cases} \quad (13)$$

Regarding the above-mentioned equation, one can find the accelerating degradation of power semiconductors, i.e., IGBT and power diode. Each of the constant in (13) is assumed to be *normally distributed* with 5% variation for considering uncertainties. Fig. 7 demonstrates the degradation trends of IGBT and power diode and their corresponding degradation states.

3) Defining Effective Items' State Spaces: The power converter has two effective degradation processes. For each of them,

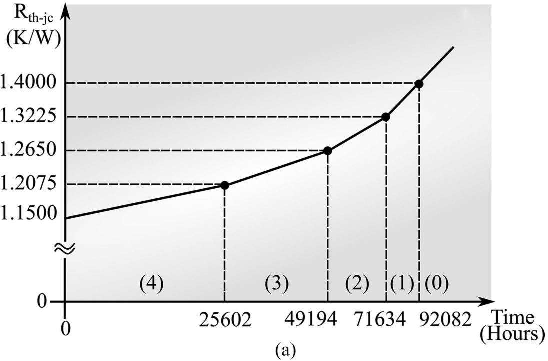

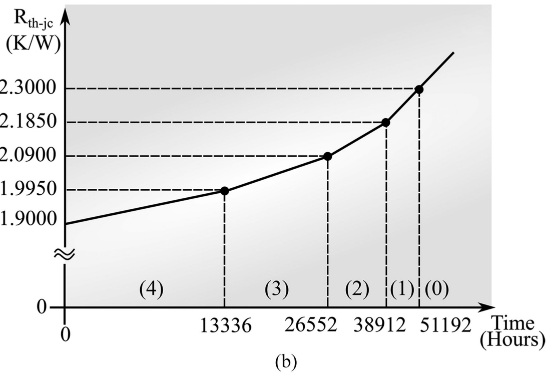

Fig. 7. Degradation processes of (a) IGBT and (b) power diode.

five different discrete states have also been taken into account. Their state spaces are denoted by $\Omega_{\mathbf{1}} = \{4_1, 3_1, 2_1, 1_1, 0_1\}$ and $\Omega_{\mathbf{2}} = \{4_2, 3_2, 2_2, 1_2, 0_2\}$. The perfect states of them are 4_1 and 4_2 and the failure states are 0_1 and 0_2. Accordingly, once either IGBT or power diode reaches their zero states, the system is failed.

4) Defining Effective Items' Intervals Corresponded to Their State Spaces: Y $_1(t)$ and $Y_2(t)$ fall into predefined intervals corresponding to their five intermediate degradation states. Since 20% increase in the junction to case thermal resistance has been considered as the failure criterion, 5% step increase in the junction to case thermal resistance is considered for discretizing the degradation trend to five intermediate states for both IGBT and power diode. Let consider the intervals as follows: $\{[1, 1.05], (1.05, 1.1], (1.1, 1.15], (1.15, 1.2], (1.2, \infty)\} \times R_{\text{th'nominal}}$. Nominal junction to case thermal resistances of IGBT and diode are 1.16 °C/W and 1.9 °C/W, respectively.

Therefore

$$\begin{aligned} 0 < Y_1(t) \leq 1.2075 & \quad \Rightarrow \quad 4_1 \\ 1.2075 < Y_1(t) \leq 1.265 & \quad \Rightarrow \quad 3_1 \\ 1.265 < Y_1(t) \leq 1.3225 & \quad \Rightarrow \quad 2_1 \\ 1.3225 < Y_1(t) \leq 1.4 & \quad \Rightarrow \quad 1_1 \\ G_1 = 1.4 < Y_1(t) & \quad \Rightarrow \quad 0_1 \end{aligned}$$

and

$$\begin{aligned} 0 < Y_2(t) \leq 1.995 & \quad \Rightarrow \quad 4_2 \\ 1.995 < Y_2(t) \leq 2.09 & \quad \Rightarrow \quad 3_2 \\ 2.09 < Y_2(t) \leq 2.185 & \quad \Rightarrow \quad 2_2 \\ 2.185 < Y_2(t) \leq 2.3 & \quad \Rightarrow \quad 1_2 \\ G_2 = 23 < Y_2(t) & \quad \Rightarrow \quad 0_2. \end{aligned} \quad (14)$$

5) Defining System State Space and Mapping Matrix: The power system state space is assumed as $\boldsymbol{\Omega}_U = \{4, 3, 2, 1, 0, F\}$ consisting six distinct states. Assuming that at time *t*, the system is not in its catastrophic failure state (*F*), one can assume $\boldsymbol{\Omega} = \{4, 3, 2, 1, 0\}$ instead of $\boldsymbol{\Omega}_U$. Mapping matrix of following equation is also assumed:

$$H_c = \begin{array}{c} \\ 0_1 \\ 1_1 \\ 2_1 \\ 3_1 \\ 4_1 \end{array} \begin{array}{c} \begin{array}{ccccc} 0_2 & 1_2 & 2_2 & 3_2 & 4_2 \end{array} \\ \begin{bmatrix} \times & 0 & 0 & 0 & 0 \\ 0 & 0 & 1 & 1 & 1 \\ 0 & 1 & 2 & 2 & 2 \\ 0 & 1 & 2 & 3 & 3 \\ 0 & 1 & 2 & 3 & 4 \end{bmatrix} \end{array}. \tag{15}$$

Accordingly, one can numerate *R* as

$$\left\{ \begin{array}{l} (0_1, 1_2), (0_1, 2_2), (0_1, 3_2), (0_1, 4_2), (1_1, 0_2), (1_1, 1_2), \\ (1_1, 2_2), (1_1, 3_2), (1_1, 4_2), (2_1, 0_2), (2_1, 1_2), (2_1, 2_2), \\ (2_1, 3_2), (2_1, 4_2), (3_1, 0_2), (3_1, 1_2), (3_1, 2_2), (3_1, 3_2), \\ (3_1, 4_2), (4_1, 0_2), (4_1, 1_2), (4_1, 2_2), (4_1, 3_2)(4_1, 4_2) \end{array} \right\}. \tag{16}$$

Regarding H_c and the global system state space, there are five different categories as follows:

$$R_0 = \left\{ \begin{array}{l} (0_1, 1_2), (0_1, 2_2), (0_1, 3_2), (0_1, 4_2), (1_1, 0_2), \\ (2_1, 0_2), (3_1, 0_2), (4_1, 0_2), (1_1, 1_2) \end{array} \right\}$$

$$R_1 = \{(1_1, 2_2), (1_1, 3_2), (1_1, 4_2), (2_1, 1_2), (3_1, 1_2), (4_1, 1_2)\}$$

$$R_2 = \{(2_1, 2_2), (2_1, 3_2), (2_1, 4_2), (3_1, 2_2), (3_1, 4_2)\}$$

$$R_3 = \{(3_1, 3_2), (3_1, 4_2), (4_1, 3_2)\}$$

$$R_4 = \{(4_1, 4_2)\}$$

$$R = \bigcup_{m=0}^{4} R_i. \tag{17}$$

It is seen from (16) and (17) that the function which is in the charge of mapping items' degradation states to the global system state space is a monotonic nondecreasing function. It means that if the degradation states of effective items or their combinations thereof decrease, the degradation states of the global system also either decreases or is equal to its previous state. As an example, $f(4_1, 4_2)$ is greater than $f(3_1, 4_2)$, $f(4_1, 3_2)$, and $f(3_1, 3_2)$

$$f\,(4_1, 4_2) = 4 > f\,(3_1, 4_2) = f\,(4_1, 3_2) = f\,(3_1, 3_2) = 3.$$

6) Reliability Assessment of by Estimating Nonfailure States' Probabilities: In this case study, power capacitor is considered as an ineffective item with following time to failure distribution [40]:

$$D\,(t; \eta, \beta)\ \sim W(1471680, 1.93). \tag{18}$$

A power capacitor has been assumed to be failed whenever its unreliability reach 10% (B_{10}). The probability density function and mean time to failure will be obtained on the state probabilities mentioned. The probability of being in state $M = 4$ would be calculated as follows:

$$P_t(4) = P(f(R_4)) = P(0 < Y_1(t) < W_{4_1} \cap 0 < Y_2(t) < W_{4_2}) \times\ P(D(t) < B_{10}). \tag{19}$$

Since the degradation processes are assumed to be independent, one can find that

$$\begin{aligned} P_t(4) &= P(0 < Y_1(t) < W_{4_1}) \times P(0 < Y_2(t) < W_{4_2}) \\ &= \{P(Y_1(t) < W_{4_1}) - P(Y_1(t) < 0)\} \\ &\quad \times\ \{P(Y_2(t) < W_{4_2}) - P(Y_2(t) < 0)\} \\ &\quad \times\ (1 - F(t; \eta, \beta)) \end{aligned} \tag{20}$$

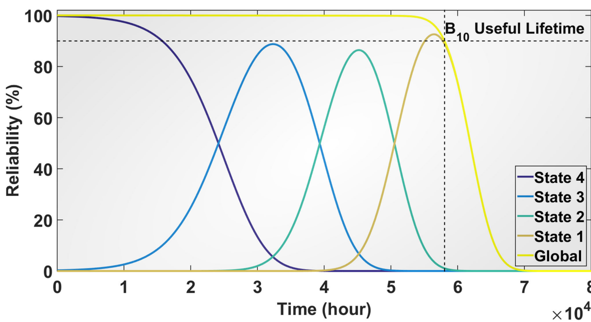

Fig. 8. Reliability functions.

where W_{41} and W_{42} are threshold values of the fourth intermediate state and are 1.2075 and 1.995 °C/W, respectively. Since $Y_i(t) = a_i + b_i t$ where $a_i \sim N(\mu_{ai}, \sigma_{ai}^2)$ and $b_i \sim N(\mu_{bi}, \sigma_{bi}^2)$, $Y_i(t)$ will follow normal distribution as follows:

$$\begin{aligned} &Y_i(t) \sim N(\mu_{ai} + \mu_{bi} t, \sigma_{ai}^2 + t^2 \sigma_{bi}^2)\,, \quad i = 1, 2 \\ &\mu_i = \mu_{ai} + \mu_{bi} t \\ &\sigma_i = \sigma_{ai}^2 + t^2 \sigma_{bi}^2. \end{aligned} \tag{21}$$

Therefore, one can calculate the following:

$$P_t(4) = \Phi\left(\frac{W_{4_1} - \mu_1}{\sigma_1}\right) \times \Phi\left(\frac{W_{4_2} - \mu_2}{\sigma_2}\right) \times\ (1 - F(t; \eta, \beta))\,. \tag{22}$$

The other system states probablities can also be estimated in the same procedure described in (19)–(22). Fig. 8 illustrates the reliability of the different system states. Since the coefficients have been assumed to be normally distributed, the system probability is also normally distributed. The yellow curve shows the reliability of the global system. Unreliability of 10% or 90% reliability (B_{10}) is achieved at 58 040 h. Accordingly, the power electronic system may work over 58 040 with 90% reliability. Based on the conventional PoF-based reliability assessment approach, the reliability of this system is about 66 680 h. It means that by considering the mutual and self-degradation effects, the reliability evaluation of the system is much more realistic.

V. Conclusion

In this article, a new reliability assessment framework has been proposed. Based on this method, the operating condition of a system has been characterized by a finite number of degraded states. This leads to the consideration of the dependance of components' aging on the operating condition which finally leads to much more realistic reliability assessment.

The items of a system have been categorized into two different items, effective and ineffective items. Effective items are those that directly affect the operating condition of the system. While ineffective items do not make meaningful contribution on the operating condition of the system and their failures lead to the catastrophic failure of the systems. Degradation processes of the effective items have been extracted from the mission profile based on the aging tests and have been divided into several

intermediate degraded states. The various combinations of the effective items' states have been mapped to the global system states using a mapping matrix.

The proposed framework has been applied to a power electronic system containing two effective components, namely IGBT and diode, and one ineffective item, namely power capacitor. Mission profile based aging tests have been performed to study the degradation processes of IGBT and power diode. The results showed that the power electronic system which was exposed to the WLTP-class3 driving cycle might work over 58 040 h by 90% reliability.

An experimental work must be planned in the future to validate the estimated lifetimes using the proposed method. However, using the present results, it appears from this article that it is very important to take into account the degradation dependencies for calculating the lifetime of the power electronic converters. This new method could be a good option to answer this issue.

References

[1] D. Zhou, Y. Song, Y. Liu, and F. Blaabjerg, "Mission profile based reliability evaluation of capacitor banks in wind power converters," *IEEE Trans. Power Electron.*, vol. 34, no. 5, pp. 4665–4677, May 2019.

[2] S. Ashrafi and S. Zarezadeh, "A shock-based model for the reliability of three-state networks," *IEEE Trans. Rel.*, vol. 67, no. 1, pp. 274–284, Mar. 2018.

[3] Y.-H. Lin, Y.-F. Li, and E. Zio, "A comparison between Monte Carlo simulation and finite-volume scheme for reliability assessment of multi-state physics systems," *Rel. Eng. Syst. Saf.*, vol. 174, pp. 1–11, 2018.

[4] M. Andresen, K. Ma, G. Buticchi, J. Falck, F. Blaabjerg, and M. Liserre, "Junction temperature control for more reliable power electronics," *IEEE Trans. Power Electron.*, vol. 33, no. 1, pp. 765–776, Jan. 2018.

[5] F. Blaabjerg, D. Zhou, A. Sangwongwanich, and H. Wang, "Design for reliability in renewable energy systems," in *Proc. Int. Symp. Power Electron.*, 2017, pp. 1–6.

[6] Y. Hu, Y. Ding, F. Wen, and L. Liu, "Reliability assessment in distributed multi-state series-parallel systems," *Energy Procedia*, vol. 159, pp. 104–110, 2019.

[7] W. Dong, S. Liu, L. Tao, Y. Cao, and Z. Fang, "Reliability variation of multi-state components with inertial effect of deteriorating output performances," *Rel. Eng. Syst. Saf.*, vol. 186, pp. 176–185, 2019.

[8] W. Li and M. J. Zuo, "Reliability evaluation of multi-state weighted k-out-of-n systems," *Rel. Eng. Syst. Saf.*, vol. 93, no. 1, pp. 160–167, 2008.

[9] S. Eryilmaz, "A reliability model for a three-state degraded system having random degradation rates," *Rel. Eng. Syst. Saf.*, vol. 156, pp. 59–63, 2016.

[10] Y. Sun, T. Sun, M. G. Pecht, and C. Yu, "Computing lifetime distributions and reliability for systems with outsourced components: A case study," *IEEE Access*, vol. 6, pp. 31359–31366, 2018.

[11] Y. Liu and C.-J. Chen, "Dynamic reliability assessment for nonrepairable multistate systems by aggregating multilevel imperfect inspection data," *IEEE Trans. Rel.*, vol. 66, no. 2, pp. 281–297, Jun. 2017.

[12] V. Kumar, L. Singh, and A. K. Tripathi, "Reliability analysis of safety-critical and control systems: A state-of-the-art review," *IET Softw.*, vol. 12, no. 1, pp. 1–18, 2018.

[13] Y. Liu, Y. Chen, and T. Jiang, "On sequence planning for selective maintenance of multi-state systems under stochastic maintenance durations," *Eur. J. Oper. Res.*, vol. 268, no. 1, pp. 113–127, 2018.

[14] X. Zhao, S. Wang, X. Wang, and K. Cai, "A multi-state shock model with mutative failure patterns," *Rel. Eng. Syst. Saf.*, vol. 178, pp. 1–11, 2018.

[15] Y.-H. Lin, Y.-F. Li, and E. Zio, "Reliability assessment of systems with dependent degradation processes based on piecewise-deterministic Markov process BT," in *Recent Advances in Multi-State Systems Reliability: Theory and Applications*, A. Lisnianski, I. Frenkel, and A. Karagrigoriou, Eds. Cham, Switzerland: Springer, 2018, pp. 213–225.

[16] Y. Lin, Y. Li, and E. Zio, "A reliability assessment framework for systems with degradation dependency by combining binary decision diagrams and Monte Carlo simulation," *IEEE Trans. Syst., Man, Cybern., Syst.*, vol. 46, no. 11, pp. 1556–1564, Nov. 2016.

[17] W. Wang, F. Di Maio, and E. Zio, "Three-loop Monte Carlo simulation approach to multi-state physics modeling for system reliability assessment," *Rel. Eng. Syst. Saf.*, vol. 167, pp. 276–289, 2017.

[18] X. Zhao, C. Wu, S. Wang, and X. Wang, "Reliability analysis of multi-state k-out-of-n: G system with common bus performance sharing," *Comput. Ind. Eng.*, vol. 124, pp. 359–369, 2018.

[19] B. Jafary and L. Fiondella, "A universal generating function-based multi-state system performance model subject to correlated failures," *Rel. Eng. Syst. Saf.*, vol. 152, pp. 16–27, 2016.

[20] Y. Liu, Q. Liu, C. Xie, and F. Wei, "Reliability assessment for multi-state systems with state transition dependency," *Rel. Eng. Syst. Saf.*, vol. 188, pp. 276–288, 2019.

[21] A. Lisnianski and Y. Ding, "Using inverse Lz-transform for obtaining compact stochastic model of complex power station for short-term risk evaluation," *Rel. Eng. Syst. Saf.*, vol. 145, pp. 19–27, 2016.

[22] X. Song, Z. Zhai, Y. Liu, and J. Han, "A stochastic approach for the reliability evaluation of multi-state systems with dependent components," *Rel. Eng. Syst. Saf.*, vol. 170, pp. 257–266, 2018.

[23] X. Yang, Z. Lin, J. Ding, and Z. Long, "Lifetime prediction of IGBT modules in suspension choppers of medium/low-speed Maglev train using an energy-based approach," *IEEE Trans. Power Electron.*, vol. 34, no. 1, pp. 738–747, Jan. 2019.

[24] C. D. Dao and M. J. Zuo, "Selective maintenance for multistate series systems with S-dependent components," *IEEE Trans. Rel.*, vol. 65, no. 2, pp. 525–539, Jun. 2016.

[25] V. Samavatian, Y. Avenas, and H. Iman-Eini, "Mutual and self-aging effects of power semiconductors on the thermal behaviour of DC-DC boost power converter," *Microelectron. Rel.*, vol. 88/90, pp. 493–499, 2018.

[26] S. Yang, A. Bryant, P. Mawby, D. Xiang, L. Ran, and P. Tavner, "An industry-based survey of reliability in power electronic converters," *IEEE Trans. Ind. Appl.*, vol. 47, no. 3, pp. 1441–1451, May/Jun. 2011.

[27] H. Wang and F. Blaabjerg, "Reliability of capacitors for DC-link applications in power electronic converters—An overview," *IEEE Trans. Ind. Appl.*, vol. 50, no. 5, pp. 3569–3578, Sep./Oct. 2014.

[28] S. H. Ali, S. Dusmez, and B. Akin, "Investigation of collector emitter voltage characteristics in thermally stressed discrete IGBT devices," in *Proc. IEEE Energy Convers. Congr. Expo.*, 2016, pp. 1–6.

[29] S. H. Ali, M. Heydarzadeh, S. Dusmez, X. Li, A. S. Kamath, and B. Akin, "Lifetime estimation of discrete IGBT devices based on Gaussian process," *IEEE Trans. Ind. Appl.*, vol. 54, no. 1, pp. 395–403, Jan./Feb. 2018.

[30] V. Samavatian, H. Iman-Eini, and Y. Avenas, "An efficient online time-temperature-dependent creep-fatigue rainflow counting algorithm," *Int. J. Fatigue*, vol. 116, pp. 284–292, 2018.

[31] M. Brincker, S. Söhl, R. Eisele, and V. N. Popok, "Strength and reliability of low temperature transient liquid phase bonded CuSnCu interconnects," *Microelectron. Rel.*, vol. 76/77, pp. 378–382, 2017.

[32] R. Chen *et al.*, "Improvement of low-temperature impact toughness for 304 weld joint produced by laser-MIG hybrid welding under magnetic field," *J. Mater. Process. Technol.*, vol. 247, pp. 306–314, Sep. 2017.

[33] W. Lai, M. Chen, L. Ran, O. Alatise, S. Xu, and P. Mawby, "Low ΔT_j stress cycle effect in IGBT power module die-attach lifetime modeling," *IEEE Trans. Power Electron.*, vol. 31, no. 9, pp. 6575–6585, Sep. 2016.

[34] I. F. Kovacevic, U. Drofenik, and J. W. Kolar, "New physical model for lifetime estimation of power modules," in *Proc. Int. Power Electron. Conf. ECCE Asia*, 2010, pp. 2106–2114.

[35] R. Bayerer, T. Herrmann, T. Licht, J. Lutz, and M. Feller, "Model for power cycling lifetime of IGBT modules—Various factors influencing lifetime," in *Proc. 5th Int. Conf. Integr. Power Syst.*, 2008, pp. 1–6.

[36] S. Yang, D. Xiang, A. Bryant, P. Mawby, L. Ran, and P. Tavner, "Condition monitoring for device reliability in power electronic converters: A review," *IEEE Trans. Power Electron.*, vol. 25, no. 11, pp. 2734–2752, Nov. 2010.

[37] H. Berg and E. Wolfgang, "Advanced IGBT modules for railway traction applications: Reliability testing," *Microelectron. Rel.*, vol. 38, no. 6/8, pp. 1319–1323, 1998.

[38] U. Scheuermann and S. Schuler, "Power cycling results for different control strategies," *Microelectron. Rel.*, vol. 50, no. 9/11, pp. 1203–1209, 2010.

[39] C. Durand, M. Klingler, D. Coutellier, and H. Naceur, "Power cycling reliability of power module: A survey," *IEEE Trans. Device Mater. Rel.*, vol. 16, no. 1, pp. 80–97, Mar. 2016.

[40] D. Zhou, H. Wang, and F. Blaabjerg, "Mission profile based system-level reliability analysis of DC/DC converters for a backup power application," *IEEE Trans. Power Electron.*, vol. 33, no. 9, pp. 8030–8039, Sep. 2018.